RSSI, Vol. 06, No. 01, Décembre 2016 34-43

Revue des Sciences et Sciences de l'Ingénieur

ISSN 2170-0737

Journal homepage :http://www.RSSI.lagh-univ.dz

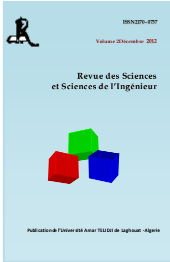

Induction Machine Diagnosis of the Broken Rotor Bars Based on Air-Gap Magnetic Flux Density

A. SEGHIOUR, T. SEGHIER, B. ZEGNINI

Laboratoire d'Étude et Développement des Matériaux Semi-Conducteurs et Diélectriques, Université Amar Telidji-Laghouat, Algérie.

Corresponding author: a.seghiour@lagh-univ.dz

Abstract: **In this paper; air-Gap magnetic flux density of induction machine is considered to detect faults such as broken rotor bars. Electrical condition monitoring using air-gap magnetic flux density and magnetic vector potential is chosen due to its effectiveness, simplicity and low cost. The magnetic field is efficient due to its ability to sample the harmonics component that consists the full information of induction machine fault via fast Fourier transform FFT. The Maxwell equations describe the local behaviour in time and space of magnetic performance. Modélisation has well done by using finite elements method in cases of a healthy and faulty machine in which used for modelling the broken rotor bars.**

Keywords: **Induction machine, Fault detection, Broken rotor bars, Finite elements method, Magnetic field.**

Résumé: **Dans cet article ; la densité du flux magnétique dans l'entre fer de la machine à induction est considéré pour détecter des éventuels défauts, tels que les barres rotoriques cassées. Cette méthode est largement utilisée pour en raison de sa efficacité et simplicité. La discrétisation du champ magnétique via la transformation FFT nous donne des informations meilleures sur la présence des défauts dans la machine. Les équations de Maxwell qui décrivent le comportement dans le temps et l'espace du champ magnétique sont à la base de la modélisation d'une machine à induction contenant des défauts. En utilisant la méthode des éléments finis une machine sans défauts et machine avec des barres rotoriques cassées sont modélisées.**

Mots-clés : **machine à induction , détection des défauts , barres de cassées , méthode des éléments finis , champ magnétique.**

I. Introduction

Rotating Induction machines (IMs) are critical tools components in the widely held of industrial application, periodical maintenance when an organised stop in the installation was set, away from each other, they have been considered as high reliable devices needful a considerable attention [1]. The importance of IMs in the productive make them be one of the most critical elements in the industrial. Such as IM faults are due to mechanical and electrical stresses. Mechanical stresses are caused by daily works of IMs, overloads, and unexpected load changes [2], which can particle results eccentricities faults and broken rotor bar. Meanwhile, electrical stresses are usually associated with the power supply disturbances, frequent starts, and operation from PWM drives, which can cause inter-turn short circuits in stator winding turns/coils closest to the motor terminal, as well as broken rotor bars and bearing problems [3]. Broken rotor bars effect of reducing machine efficiency and localised rotor heating more than this a vibration due to rotor expansion and bowing. These effects cause to thermal stresses during starting or overload, which results in mechanical (loose laminations, fabricated parts or bearing failures) and magnetic stresses (electromagnetic forces, unbalanced magnetic pulls, electromagnetic noise), also the dynamic stresses due to shaft torques.

The detection of broken rotor bars are developed during this years, many approaches have been proposed for modelling this faults, broken rotor bar fault occurred when the bar current is considered to be equal to zero for modelling broken bars [4- 6]. That mean the bar breakage increases the currents of the adjacent bars considerably. This implies a significant asymmetry in the rotor squirrel cage circuit and consequently, asymmetry in the field resulted by the rotor bars currents. Therefore, in the modelling of broken bars, for the electric circuit model of IMs, currents of bars failures are considered near to zero, in which the resistance of the broken bar is has a high value, in [7] they have been considered the resistance of the healthy IM as 39.42 $\mu\Omega$ and broken bar as 2500 $\mu\Omega$. Moreover, the Finite element model in the modelling of broken bars can be damaged progressively. First, they can be cracked, but not entirely broken by model this state with a low electrical conductivity of the corresponding bar or by high resistance in which increase the rotor bar resistance. Second, they are definitively broken by zero electrical conductivity [7, 8].

Many researchers have proposed methods for the analysis of the steady state and performance rotor bars fault [9-11]. The dynamic models give the solution as instantaneous values from which the signal components can be computed under a quasi-steady state. However, based on the previously references the most signature signal used in diagnosis broken rotor bars is the stator currents, which have dealt in the stator currents spectrum. Furthermore, the electric frequency of currents is equal to two times of mechanical frequency, in fact, the high variation of stator current more than the effect of the fault in IM especially broken rotor bar, more than this, The stator current spectrum present a weakness. Indeed many cases of unnecessary motor inspection or outage due to false alarms produced by rotor axial duct interference have been reported [12-14]. If the number of axial ducts and poles is identical, this can produce sidebands frequency around the fundamental component that overlaps with rotor faults, resulting in false alarms. However, there currently is no practical test method available for distinguishing rotor faults and false indications. The contribution of this paper as follows:

The modelling of broken rotor bars based on finite element method, by removing boundaries of failure bar that give’s the characteristics of air-gap, which mean the bar breakage domain added to air-gap. Moreover, bounded the limit conditions of a rotor bar field to the air-gap which have occurred has properties [8, 15, 16]. This method expresses the increase in rotor bar resistance; it means the cancellation of currents bars. The magnetic field signature analysis (MFSA) is proposed to detect faults, that has the full information about the machine functioning, it is possible and easy to predict and diagnosis all faults by monitoring of the air-gap magnetic flux density, also this paper discusses the investigation the effect of broken rotor bars position, in which have proposed many states for this type of faults. Due to the many start and stop of IM the possibility of change location broken bars is present, we deal with two forms of location bars firstly at zero degree then at 180 degrees is considered. Identification of faults was made by the air-gap magnetic flux density spectrum when machines operating in no-load conditions or at low slip is presented.

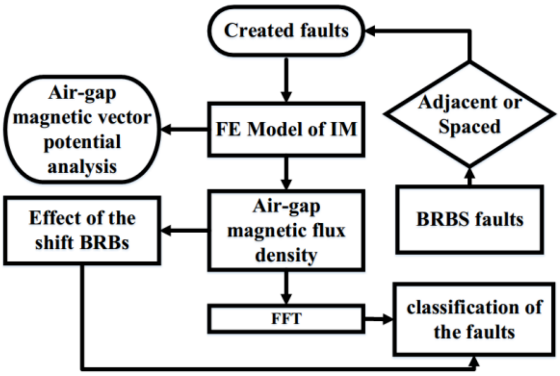

Fig .1: Diagram of proposed analysis

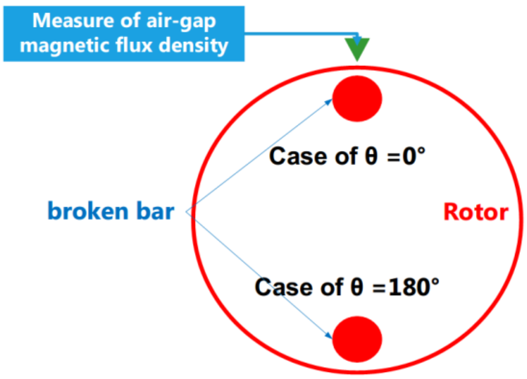

Fig .2: The location cases of broken rotor bars.

II. Methodology

IMs are physically composed of a squirrel cage rotor. The rotor is the most inner part of the IM, the rotation of electromagnetic field induced in its coils from the stator field. Due to the quite large types and applications of squirrel cage rotor, the focus of this paper is on the squirrel cage IMs, in which this kind of machine has an active rotor. However, rotor faults such as broken bar are absorbing diagnosis problem. The primary technique used in this analysis based on magnetic field diagnosis, in which used the FEM to create BRBs faults, in this paper, we deal with adjacent and spaced rotor bars faults. That takes two forms; when the measurement of air-gap magnetic flux density for shifting by angle 0 and also for 180. Moreover, the location of the faults it can exist near or far from the point of measure. Figure 1 shows the proposed fault detection and diagnosis based on finite element method, which used for modelling IM and for creating broken rotor failures. The methods of the arc length of the air-gap magnetic vector for analysing the locating rotor bars faults. The air-gap magnetic flux density during the normal condition of an IM varies sinusoidally both in space and time, and any asymmetries in the stator or rotor may cause deviations of such sinusoidal variation. Due to the sinusoidal form of air-gap magnetic flux density, a Fast Fourier Transform (FFT) is used for identifying the broken rotor bars in two cases (Figure 2 presented the two forms of location rotor bar faults).

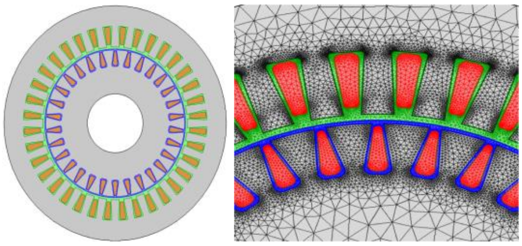

(a) (b)

Fig .3: Geometry and meshing model of machine, (a) geometry, (b) Mesh

III. FEM induction machine model

Geometry and parameters of machine

FEM is used for the magnetic field calculation. The two-dimensional (2D) field calculations are performed using Maxwell's equations. For pre-processing stage of FEM calculation the physical properties, real geometry is required. The mesh generation is also an important point, the 2D of Geometry and Mesh for Squirrel-Cage Induction Machine presented in Figure. 3, the parameters of studied machine in this work is provided in the Table. I.

Table 1 Machine Parameters

Variable	Value
Number of poles	4
Number of phases	3
Rated voltage (V)	220
Rated frequency (Hz)	50
Rotation speed (rpm)	1500
Number of stator slots	36
Number of rotor slots	30
Outer diameter of the motor core (m)	0.12
Inner diameter of the motor core (m)	0.075
Air Gap length (m)	0.003
Slip	0.000114

Electromagnetic Field Equations

In 2D analysis using Magnetic vector potential A_z , the governing equations of eddy current problem are acquired from Maxwell equations neglecting the displacement current in Eq. (2) will be rewriting by the Eq. (6) where Electric field intensity E, Electric displacement or electric flux density D, Magnetic field intensity H, Magnetic flux density B, Current density J.

$$\nabla \times E = -\frac{\partial B}{\partial t} \qquad (1)$$

$$\nabla \times H = J + \frac{\partial D}{\partial t} \qquad (2)$$

$$\nabla \cdot B = 0 \qquad (3)$$

For conductive layers, either stationary or moving with velocity vector , the induced current is accounted for using Ohm's law for moving regions, J is defined by:

$$J = \sigma E + \sigma v \times B + J_e \qquad (4)$$

Where Je is an externally current density, and ν is the velocity of the conductor and σ the electrical conductivity. Applying the definition of the magnetic vector potential.

$$B = \nabla \times A \qquad (5)$$

The variation of electric displacement will be zero by Quasistatic analysis of Maxwell-Ampere equation becomes

$$\nabla \times H = J \qquad (6)$$

The resulting electromagnetic field equation for conductive layers, found by applying Eq.(1) to Eq.(6), the general equation is given by;

$$\sigma \frac{\partial A}{\partial t} + \nabla \times \left(\mu_0^{-1} \mu_r^{-1} \nabla \times A \right) - \sigma v \times \nabla \times A = J_e \qquad (7)$$

The stator winding is composed of multi-turn coils the component of the current density in the direction of the wires is defined as $J_e = \frac{N(V_{A,B,C} + V_{ind})}{A_{winding} \cdot R_{A,B,C}}$, by applied in the winding currents equilibrium for each phase shapes 3π/2 radian. where $V_{A,B,C}$ are the voltages applied to the three stator slots, J_e is the current generated by the stator windings, $A_{winding}$ is the cross section of the winding domain, N is the number of turns of a stator winding, $R_{A,B,C}$ the stator resistances, V_{ind} is the induced voltage calculated by integrating the electric field along the coil of stator winding.

The cage windings areaway of short circuit $(V_r = 0)$ the rotor voltages equals to zero. They producing by the effect of induction created by stator windings. The number of poles pairs does not affect by the effect of induction coming from the stator. The rotor bar is composed of single turn coil; the out-of-plane component of the current density is defined as:

$$J_e = \frac{\sigma V_{ind}}{A_{bar} \cdot R_{a,b,c}} \qquad (8)$$

where $R_{a,b,c}$ is the rotor resistance, A_{bar} is the cross section of the rotor bar domain.

The modelling motion of rotating electrical machines is made by displacement mesh, where the moving mesh will be done to the rotor and the part of the rotoric-air-gap. On the other side, the stator and the rest part of the air gap are fixed [16]. However, the material used for the machine structure and ferromagnetic type soft iron (without loss). As relationship, nonlinear characteristic, that associates the magnetic flux density B and the magnetic field H. Figure 3 shows the $B-H$ curve of this type of material. Therefore, it can be seen that soft iron reaches its best state of magnetization near saturation between 1.6 Tesla and 2.4 Tesla, and supersaturation should be avoided.

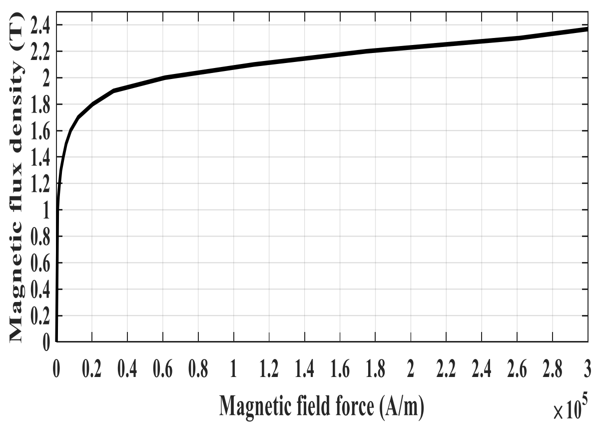

Fig. 4: $B-H$ curve.

IV. Model of IM with rotor fault

The proposed model of induction machine based to remove the rotor bar domain, which added to the rotoric air-gap, moreover, in the geometry of induction machine create unbalanced in the squirrel cage of the rotor, Figure 5 show the geometry and mesh of faulty machines containing a rotor bar fault. The number of triangular elements should reduce by increasing the number of broken rotor bars. Table 2 presented the number of triangular elements in the air-gap, according to the state of the machine. The broken rotor bars can happen in any position in the squirrel cage, and the break of the bar can be adjacent or spaced. Hence, we propose some many possibilities as shown in Figure 5. the proposed broken rotor bars in this work as follows:

1. One broken rotor bar.
2. Three adjacent broken rotor bars.
3. Three spaced broken rotor bars by the angle of 120 degrees.

Then, we deal with the same faults in which shift all rotor bars by the angle of 180 degrees as presented in Figure 2.

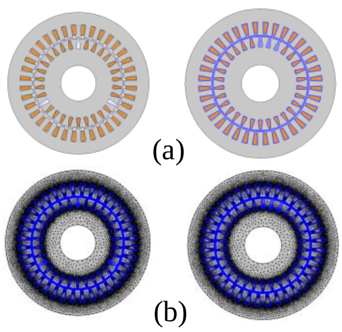

Fig. 5: Faulty machine with broken bar (a) geometry (b) mesh.

Table 2 Mesh comparison between healthy and faulty machine

State of machine	Air-gap Triangular number
Healthy	29405
1BRB	29273
2BRB	29150
3BRB	29018

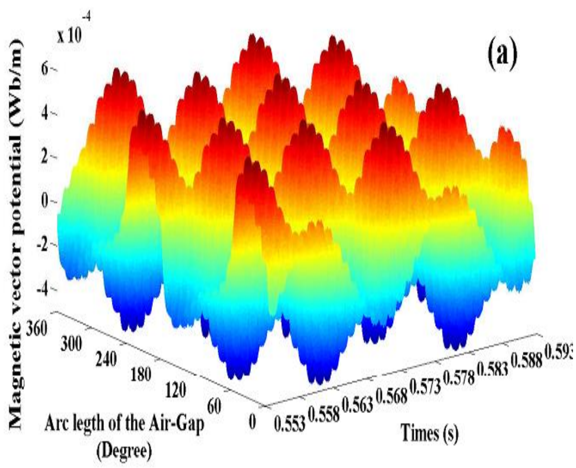

Fig. 6: Air-gap Magnetic vector potential for healthy.

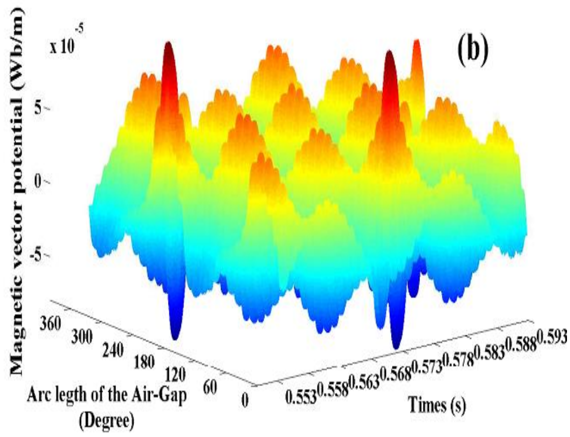

Fig. 7: Air-gap Magnetic vector potential for faulty machine containing one broken bar.

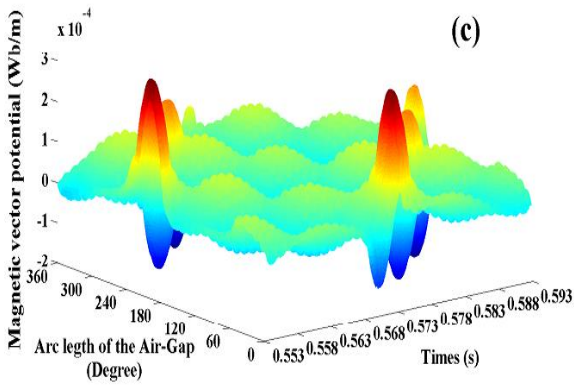

Fig. 8: Air-gap Magnetic vector potential for faulty machine containing three adjacent broken bars.

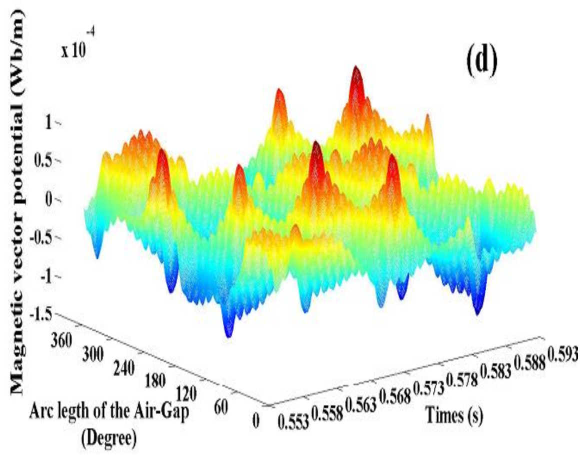

Fig. 9: Air-gap Magnetic vector potential for faulty machine containing three spaced broken bars.

In this part, present magnetic vector potential along the air-gap at the time, for the broken state one and three adjacent, spaced rotor bars, where the located of faults can be defined by increase a deep zone in the magnetic vector potential. In which have more broken bars and more increase that gives the reference position of broken bars. For broken spaced rotor bars in deformation in the amplitude of present magnetic vector potential in agreement with the distribution of broken rotor bars in the map of the rotor. Figures 6, 7, 8, and 9 show the variety of magnetic vector potential in the air-gap for broken rotor bars, which have a more broken bar more increasing of the amplitude during the time.

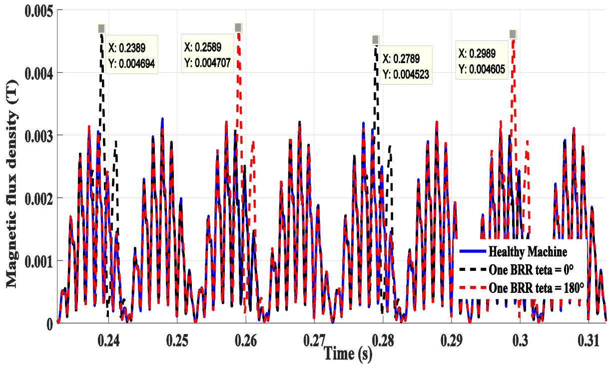

Fig. 10: Air-gap magnetic flux density for healthy and faulty IM containing One BRB.

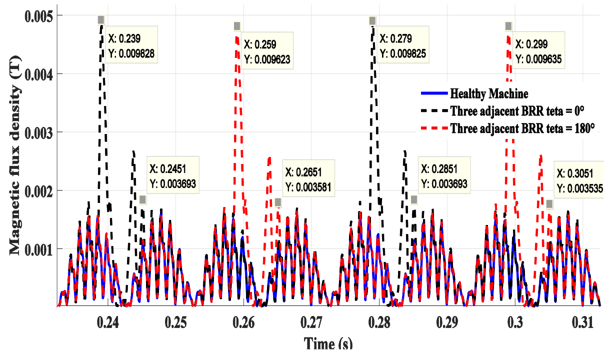

Fig. 11: Air-gap magnetic flux density for healthy and faulty IM containing Three adjacent BRBs.

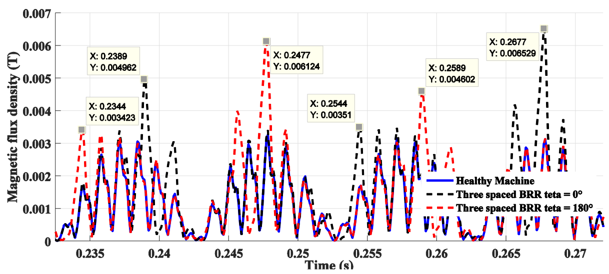

Fig. 12: Air-gap magnetic flux density for healthy and faulty IM containing Three spaced BRBs.

V. Air-gap magnetic flux density analysis

The general equation of IM presented by the variable Az (Is the magnetic vector potential) J is the current density, which is equal to zero for steel and air parts, the magnetic flux density components, Bx and By In the x and y-axis directions, are stated as below:

$$B_x = \frac{\partial A_z}{\partial y} \qquad B_y = \frac{\partial A_z}{\partial x} \tag{9}$$

The magnetic flux density B is determined from below equation;

$$B = \sqrt{B_x^2 + B_y^2} \tag{10}$$

The 2D electromagnetic field results are employed in the present paper to determine the impact of faults in air-gap, in the magnetic field simulation with healthy rotor, one broken bar and three adjacent/spaced broken bars, also broken shifting bars. The results of magnetic flux density in the air-gap for the induction machine, which have a healthy rotor and broken rotor bars that are damaged. Figure 10, 11 and 12 show the results of calculating air-gap magnetic flux density, that shows for broken rotor bars state. One can notice that the flux density change is periodic and calm on the condition of healthy rotor, however, the flux density fluctuations with time after broken bar fault. The increase in the amplitude due to faults are very significant with the increase of broken number bars. Also the cancel of rotor bar current increase the rotor bars adjacent considerably. Moreover, the effect of one BRB increase air-gap magnetic flux density to 0.004 T as well for three adjacent BRBs to 0.009 T and 3 spaced BRBs to 0.005 T this deformation is from 0.2389 s to 0.2789 s, all this is repeated for all mechanical frequency. A comparison of Air-gap magnetic flux density plot between the healthy rotor and the broken bars fault demonstrates the harmonic components of the flux density on the different positions for broken bars are greater than those for healthy rotor.

VI. Spectral Analysis of the Magnetic Flux Density

The air gap magnetic flux density and stator currents have considerable and effects on each other, investigation of the air gap magnetic flux density are necessary as one of the sufficient signatures to detect the broken rotor bars. Any abnormal functioning of the IM increases the oscillation of electromagnetic torque and speed of machine which increases the distortion on air gap magnetic flux density. Therefore, the decrease in load causes an increase in the amplitude of side-band components around the fundamental harmonic.

$$f_{BRB} = (1 \pm 2s) f_s \tag{11}$$

The proposed technique shows efficacy in this work, which can identify the number and the type of broken rotor bars. More than this, it can detect the location of fault however concerning the point of measured. The sidebands around the fundamental frequency is present as follows:

$$f_{sidebands} = \frac{(1-s)}{p} f_s \tag{12}$$

$$\begin{aligned} f_{s_L} &= k \cdot (f_s - f_{sidebands}) \\ f_{s_U} &= k \cdot (f_s + f_{sidebands}) \end{aligned} \tag{13}$$

k : is an integer

f_s : is fundamental frequency.

$f_{sidebands}$: is the sidebands around the fundamental frequency.

s : is the slip.

p : is the pair pole.

f_{s_U} : is the frequency of the upper sidebands.

f_{s_L} : is the frequency of the lower sidebands.

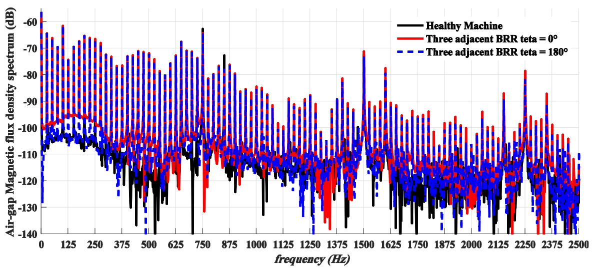

Fig. 13: Air-gap magnetic flux density spectrum for healthy and faulty IM containing One BRB.

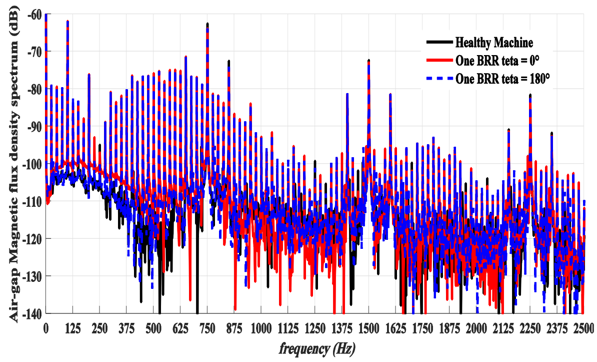

Fig. 14: Air-gap magnetic flux density spectrum for healthy and faulty IM containing Three adjacent BRBs.

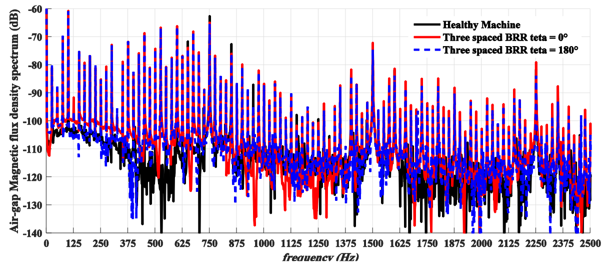

Fig. 15: Air-gap magnetic flux density spectrum for healthy and faulty IM containing Three spaced BRBs.

When a rotor bar is cracked, no current flows through it, and thus no magnetic flux generated around that bar. This occurrence generates an irregularity in the rotor magnetic field by producing a non-zero backwards rotating magnetic field. Therefore, it induces harmonic magnetics in the air-gap, which superimposed on the stator currents.

These superimposed harmonics used as signatures for BRB detection in Magnetic field signature analysis. The frequency spectrum of the air-gap magnetic flux density exposes sideband components f s L and f s U around the fundamental components in the presence of the BRB.

According to Table.3, at the frequency of the sidebands increases from -99 to -76 dB for one broken bar rated to healthy IM. Also -64 to -74 dB for three adjacent bars and from -70 to -98 dB for three spaced rotor bars. More broken bars more increase in the amplitude of the sidebands components in case of adjacent bars, another side, the effect of spaced broken rotor bars is lower than adjacent due to the distribution force in the rotor core.

Table 3 Air-gap magnetic flux density spectrum of induction machine around fundamental frequency.

rank	f_s	angle	healthy f_{sL}	healthy f_{sU}	1BRB f_{sL}	1BRB f_{sU}	3BRB f_{sL}	3BRB f_{sU}	3BRBS f_{sL}	3BRBS f_{sU}
1	49.99	0	-103.15	-103.34	-79.17	-81.03	-64.25	-69.54	-80.93	-70.05
		180			-78.42	-79.64	-64.22	-69.25	-80.06	-69.68
3	149.97	0	-103.21	-105.74	-84.53	-87.91	-74.21	-67.15	-91.53	-79.11
		180			-82.09	-88.29	-73.42	-67.24	-96.68	-80.01
5	249.95	0	-103.32	-107.03	-92.92	-88-87	-65.94	-67.88	-80.99	-80.51
		180			-99.27	-88.79	-65.99	-68.15	-80.07	-81.78
7	349.94	0	-110.19	-109.35	-83.5	-80.64	-73.03	-76.33	-98.56	-71.67
		180			-83.48	-80.14	-73.24	-76.53	-95.55	-71.64
9	449.92	0	-119.14	-110.98	-78.05	-76.55	-72.46	-71.26	-75.72	-80.88
		180			-77.97	-76.08	-72.71	-71.58	-76.05	-80.56

BRB: broken rotor bar
BRBS: broken spaced rotor bars

VII. Conclusions

In this paper, it has been developed a new methodology for the diagnosis of faults in induction machines operating under no-load conditions, based on the analysis of the air-gap magnetic flux density frequency, which determines the faults in a separate way for broken rotor bars. The methodology provides a powerful diagnosis, as well as improve the accuracy and reliability of the already developed techniques used. The development of the method and results in this paper consisted of the following set of steps:

- Proposed an induction machine model based on finite element method used for creating rotor faults.
- Analysis of the faulty components of broken rotor bars in squirrel cage induction machines, in a separate way.
- The magnetic vector potential and air gap magnetic flux density are used for the diagnosis the effect of each fault.
- The power spectrum density of the air-gap magnetic flux density used for identifying proposed faults inside band components around the fundamental frequency.

The effect of one BRB increase air-gap magnetic flux density to 0.004 T as well for three adjacent BRBs to 0.009 T and 3 spaced BRBs to 0.005 T this deformation is from 0.2389 s to 0.2789 s. More broken bars more increase in the amplitude of the sidebands components in case of adjacent bars, another side, the effect of spaced broken rotor bars is lower than adjacent due to the distribution force in the rotor core.

References

[1] P. J. Tavner, “Review of condition monitoring of rotating electrical machines,” IET Electric Power Applications, vol. 2, no. 4, p. 215, 2008.

[2] J. Faiz, B. M. Ebrahimi, B. Akin, and H. A. Toliyat, “Dynamic analysis of mixed eccentricity signatures at various operating points and scrutiny of related indices for induction motors,” IET Electric Power Applications, vol. 4, no. 1, p. 1, 2010.

[3] R. Valles-novo, J. D. J. Rangel-magdaleno, J. M. Ramirez-cortes, S. Member, H. Peregrina-barreto, and R. Morales-caporal, “Empirical Mode Decomposition Analysis for Broken-Bar Detection on Squirrel Cage Induction Motors,” IEEE Transactions on Instrumentation and Measurement, vol. 64, no. 5, pp. 1118–1128, 2015.

[4] A. A. Basil. Saied, “Fault Prediction of Deep Bar Cage Rotor Induction Motor Based on FEM,” Progress In Electromagnetics Research B, vol. 1, no. August, pp. 147–157, 2008.

[5] Z. Ling, L. Zhou, S. Guo, and Y. Zhang, “Equivalent Circuit Parameters Calculation of Induction Motor,” IEEE Transactions on Magnetics, vol. 50, no. 2, pp. 4–7, 2014.

[6] J. Faiz and B.-M. Ebrahimi, “A New Pattern for Detecting Broken Rotor Bars in Induction Motors During Start-Up,” IEEE Transactions on Magnetics, vol. 44, no. 12, pp. 4673–4683, Dec. 2008.

[7] K. Boughrara, N. Takorabet, R. Ibtiouen, O. Touhami, and F. Dubas, “Analytical Analysis of Cage Rotor Induction Motors in Healthy, Defective, and Broken Bars Conditions,” IEEE Transactions on Magnetics, vol. 51, no. 2, pp. 1–17, Feb. 2015.

[8] A. Seghiour, T. Seghier, and B. Zegnini, “Diagnostic of the simultaneous of dynamic eccentricity and broken rotor bars using the magnetic field spectrum of the air-gap for an induction machine,” 3rd International Conference on Control, Engineering & Information Technology (CEIT), 2015, pp. 1–6.

[9] P. Shi, Z. Chen, Y. Vagapov, and Z. Zouaoui, “A new diagnosis of broken rotor bar fault extent in three phase squirrel cage induction motor,” Mechanical Systems and Signal Processing, vol. 42, no. 1–2, pp. 388–403, 2014.

[10] M. Y. Kaikaa, M. Hadjami, and A. Khezzar, “Effects of the Simultaneous Presence of Static Eccentricity and Broken Rotor Bars on the Stator Current of Induction Machine,” IEEE Transactions on Industrial Electronics, vol. 61, no. 6, pp. 2942–2942, 2014.

[11] J. Faiz, B. Mahdi, H. A. Toliyat, and W. S. Abu-elhaija, “Mixed-fault diagnosis in induction motors considering varying load and broken bars location,” Energy Conversion and Management, vol. 51, no. 7, pp. 1432–1441, 2010.

[12] C. Yang, T.-J. Kang, S. Bin Lee, J.-Y. Yoo, A. Bellini, L. Zarri, and F. Filippetti, “Screening of False Induction Motor Fault Alarms Produced by Axial Air Ducts Based on the Space-Harmonic-Induced Current Components,” IEEE Transactions on Industrial Electronics, vol. 62, no. 3, pp. 1803–1813, Mar. 2015.

[13] S. Lee, J. Hong, S. Bin Lee, E. Wiedenbrug, M. Teska, and H. Kim, “Evaluation of the influence of rotor axial air ducts on condition monitoring of induction motors,” in 2012 IEEE Energy Conversion Congress and Exposition (ECCE), 2012, pp. 3016–3023.

[14] C. Yang, T.-J. Kang, D. Hyun, S. Bin Lee, J. A. Antonino-Daviu, and J. Pons-Llinares, “Reliable Detection of Induction Motor Rotor Faults Under the Rotor Axial Air Duct Influence,” IEEE Transactions on Industry Applications, vol. 50, no. 4, pp. 2493–2502, Jul. 2014.

[15] A. Seghiour, T. Seghier, and B. Zegnini, “Defects rotor identification by magnetic spectrum analyzing in a squirrel-cage asynchronous machine,” International Conference on Electrical Sciences and Technologies in Maghreb, CISTEM 2014, 2014.

[16] A. Seghiour, T. Seghier, and B. Zegnini, “Diagnostic of Rotor Faults Using Spectrum Magnetic Field for an Induction Machine,” 1st International Conference on Applied Automation and Industrial Diagnostics, (ICAAID), 2014, pp. 1–10.